ACS APPLIED MATERIALS & INTERFACES

Research Article

www.acsami.org

Carbothermal Reduction of Ti-Modified IRMOF-3: An Adaptable Synthetic Method to Support Catalytic Nanoparticles on Carbon

Jongsik Kim,‡ Nicholas D. McNamara,‡ Theresa H. Her, and Jason C. Hicks*

Department of Chemical and Biomolecular Engineering, University of Notre Dame, 182 Fitzpatrick Hall, Notre Dame, Indiana 46556, United States

Supporting Information

ABSTRACT: This work describes a novel method for the preparation of titanium oxide nanoparticles supported on amorphous carbon with nanoporosity (Ti/NC) via the post-synthetic modification of a Zn-based MOF with an amine functionality, IRMOF-3, with titanium isopropoxide followed by its carbothermal pyrolysis. This material exhibited high purity, high surface area (>1000 m^2/g), and a high dispersion of metal oxide nanoparticles while maintaining a small particle size (~4 nm). The material was shown to be a promising catalyst for oxidative desulfurization of diesel using dibenzothiophene as a model compound as it exhibited enhanced catalytic activity as compared with titanium oxide supported on activated carbon via the conventional incipient wetness impregnation method. The formation mechanism of Ti/NC was also proposed based on results obtained when the carbothermal reduction temperature was varied.

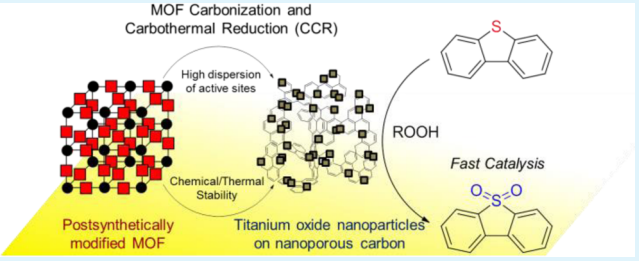

KEYWORDS: *carbonization, carbothermal reduction, incipient wetness impregnation, postsynthetic modification, metal organic framework, oxidative desulfurization*

1. INTRODUCTION

Carbon materials have been touted as excellent catalyst supports because of their high chemical (acid and base resistant) and thermal (>1000 K) stabilities.[1−4] There are a number of different methods for dispersing active metal sites on carbon including incipient wetness impregnation,[5] precipitation−deposition,[6] electrochemical deposition,[7] photochemical reduction,[8] sonochemical-assisted deposition,[9,10] and direct thermal decomposition.[11] These methods, however, frequently result in poor metal dispersion due to poor solvent−carbon support interactions as well as pore blocking.[1,6]

Metal organic frameworks (MOFs), much like carbon-supported metals, are a class of organic/inorganic hybrid materials that have received increased attention due to their various practical applications.[12−19] MOFs haved been used as catalysts in particular because of their high dispersion of active sites, well-defined structures, microporosity, and tunable physicochemical properties (via the alteration of metal atoms/ligands).[20−24] Furthermore, the postsynthetic modification of MOFs containing certain functional groups (e.g., −OH,[25,26] $-NH_2$,[27] and pyridine[28]) with organic and/or inorganic compounds has led to increased promise in practical applications.[29] This is in part due to the high dispersions of organic/inorganic compounds attainable through coordination chemistry.[25] In catalysis, however, the chemical and thermal stability of postsynthetically modified MOFs limits their recyclability, frequently resulting in structural degradation and significant leaching of active metal sites.[23,25,26,30,31] To overcome this obstacle and impart high stability, we can use MOFs as templates for the formation of various carbon-support materials.[32−35]

Using the ability to form strong coordination between the active metal precursor and the unique and diverse chemical functionalities incorporated in MOFs, we envisioned a method to, in one step, carbonize and carbothermally reduce the material, resulting in a material that retained the high surface area and high dispersion of active metal sites inherent to a postsynthetically modified MOF, while imparting the high chemical and thermal stability of carbon-supported materials (Figure 1). This method entailed the carbonization of a postsynthetically modified MOF while performing a carbothermal reduction of a coordinated metal compound (CCR). Additionally, with this method, the physicochemical properties of the carbonaceous material with high surface area can be manipulated by the alteration of the type of MOF and coordinated metal precursor during postsynthetic modification. Furthermore, the oxidation state of the metal nanoparticles can be controlled by varying the CCR temperature.

Herein, we report the synthesis of a Ti-based nanocatalyst and the catalytic properties of this material in the oxidation of dibenzothiophene (DBT). The titanium oxide particles were supported on nanoporous carbon (Ti/NC) via the post-synthetic modification of IRMOF-3 (a Zn-MOF) with titanium isopropoxide ($Ti(O\text{-}iPr)_4$), followed by CCR. Although a Ti

Received: September 20, 2013
Accepted: October 10, 2013
Published: October 10, 2013

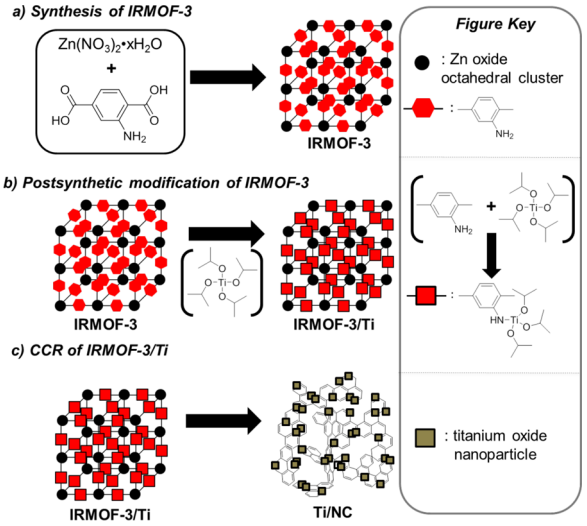

Figure 1. Schematic representation for (a) synthesis of IRMOF-3,(b) synthesis of Ti-postsynthetically modified IRMOF-3, and (c) the preparation of Ti/NC resulting from the CCR method. In Ti/NC, various defects including electronically unsaturated carbon sites and/or functional groups were omitted for simplicity.

precursor was subjected to carbonization in this work, it is easy to envision applying the CCR method to any number of other postsynthetically modified MOFs to create a new class of carbonaceous materials with high surface area.

2. EXPERIMENTAL SECTION

The following materials were purchased commercially and used as received: $Zn(NO_3)_2{\cdot}xH_2O$ (Alfa Aesar, 99%, metal basis), 2-aminoterephthalic acid (Alfa Aesar, 99%), N,N-dimethylformamide (DMF, EMD, ACS grade), $Ti(O\text{-}iPr)_4$ (Acros), activated carbon (DARCO, −100 mesh particle size, Sigma-Aldrich), decane (TCI America), dodecane (TCI America), dibenzothiophene (Alfa Aesar), and tert-butyl hydroperoxide (5.0−6.0 M in decane) (Sigma Aldrich). Chloroform (Alfa Aesar, ACS grade) and toluene (Macron, ACS grade) were thoroughly dried prior to use with 4 Å molecular sieves and Na/benzophenone, respectively.

2.1. Synthesis. *2.1.1. Synthesis of IRMOF-3.* IRMOF-3 was synthesized based on a modified procedure reported by Eddaoudi et al.[36] Approximately, 22.9 mmol of $Zn(NO_3)_2{\cdot}xH_2O$ (Alfa Aesar, 99%, metal basis) and 8.28 mmol of 2-aminoterephthalic acid (Alfa Aesar, 99%) were dissolved in 200 mL of N,N-dimethylformamide (DMF, EMD, ACS grade). The solution was heated to 105 °C overnight. After being cooled to room temperature, the reactant mixture was decanted, and the remaining brown-amber crystals were washed with fresh DMF several times. The material was then soaked in fresh DMF for stable storage. The unmodified IRMOF-3 was obtained after desolvation inside a tube furnace (He, 0.5 °C/min, 10 mL/min, 120 °C for 3 h followed by 170 °C for 6 h).

2.1.2. Postsynthetic Modification of IRMOF-3 with Ti(O-iPr)$_4$. Postsynthetically modified IRMOF-3 with $Ti(O\text{-}iPr)_4$ (IRMOF-3/Ti) has been obtained following a method slightly modified from previous studies.[25,26] In a flask, 1.046 g of $Ti(O\text{-}iPr)_4$ (Acros) in 25 mL of dry chloroform solution (dehydrated using 4 Å molecular sieves) was slowly added to 1.0 g of IRMOF-3 (desolvated, 814.95 g/base unit) in 25 mL dry chloroform inside a N_2-filled glove box. The mixture was held in a glove box under a N_2 atmosphere at 25°C for 24 h. The mixture was then filtered and washed with dry chloroform several times and soaked in anhydrous toluene for stable storage. The added amount of $Ti(O\text{-}iPr)_4$ was calculated based on the theoretical number of amine functionalities in IRMOF-3 under the assumption that the structure of IRMOF-3 was intact without any defects.

2.1.3. Carbonization and Carbothermal Reduction (CCR) of IRMOF-3/Ti. This step details the preparation method for Ti/NC derived from IRMOF-3/Ti. Typically, IRMOF-3/Ti was loaded into a tube furnace (Thermo Scientific Lindbreg Blue M) and pyrolyzed under the following conditions: He flow of 30 mL/min, heated at a ramp rate of 10 °C/min to either 550 °C for 4 h (Ti/ZnO/NC) or 1000 °C for 6 h (Ti/NC). Afterwards, the Ti/NC material was cooled to room temperature under He flow.

2.1.4. Preparation of Ti/AC via Conventional Incipient Wetness Impregnation. Incipient wetness impregnation was employed for the preparation of Ti/AC, and the entire procedure was conducted in the N_2-filled glove box. In a 250 mL beaker, 0.1375 g of $Ti(O\text{-}iPr)_4$ was completely dissolved in 3.0 g of dry chloroform (dehydrated using 4 Å molecular sieves). Approximately 1 g of dehydrated activated carbon (DARCO®) was subsequently added to the mixture. After stirring, the mixture was dried at room temperature for 2 days. The solid was then loaded into tube furnace and pyrolyzed under the following conditions: He flow of 30 mL/min, heated at a ramp rate of 10 °C/min to 1000 °C for 6 h. The prepared Ti/AC was cooled to room temperature under He flow.

2.2. Catalytic Tests on the Oxidation of Dibenzothiophene. In a typical catalytic reaction, 3.5 mmol of dibenzothiophene (DBT) was added to a stirred 100 mL round-bottom flask containing solution of decane (30 mL) and dodecane (0.5 mL as internal standard). The mixture was heated to the desired temperature at which point 7.5 mmol of tert-butyl hydroperoxide (TBHP) was added. Once the solution temperature stabilized (∼1−2 min), the desired amount of catalyst (9 μmol Ti metal center) was added. Approximately 0.5 mL aliquots of reactant mixture were taken at predetermined times, transferred to a GC vial, and diluted with decane for GC analysis. Reactant solution samples were then analyzed by injection into an Agilent Technologies model 7820A gas chromatograph (GC) system with a (5%-phenyl)-methylpolysiloxane column (length of 30 m, diameter of 0.32 mm) and an flame ionization detector (FID). The temperature of the column was held at 50 °C for 3 min and then increased to 280 °C at a ramp rate of 15 °C/min. The GC injector temperature was set to 150 °C. The carrier gas stream was composed of helium and was set to a constant flow rate of 0.5 mL/min. Reactants (DBT, BT, or thiophene) were quantified using an internal standard of dodecane.

In a typical recycle reaction test, the catalyst amount was increased to 36 μmol of Ti while all other reaction conditions were kept the same as described above. After the reaction, the catalyst was collected by filtration and washed with ∼100 mL DMF and ∼150 mL chloroform. The catalyst was then dried under vacuum overnight at 40 °C. The dried catalyst was then used in subsequent recycle reactions.

2.3. Characterization. The surface area and pore volume for all prepared materials was determined via the adsorption of N_2 at 77 K using a Quantachrome NOVA 2200e. Samples were dried under 1×10^{-5} Torr dynamic vacuum at 125 °C overnight and their surface areas were estimated over the relative pressure range of $0.001 < P/P_0 < 0.1$, and $0.05 < P/P_0 < 0.3$ in order to determine Langmuir and BET surface area, respectively. X-ray diffraction (XRD) patterns were acquired using a D8 Advance Davinci diffractometer operated at 40 kV and 40 mA with monochromated CuKα radiation (λ = 1.5418 Å) and with a scan speed of 0.75 s/step and a step size of 0.02°. SEM analysis for the observation of the macroscopic morphology of the prepared samples was performed using a Magellan 400. A Bruker Tensor 27 in DRIFTS mode was used to collect FTIR measurements. A background was first collected using finely crushed and dried KBr powder. The samples were mixed with the dry KBr and scanned from 400 to 4000 cm^{-1}. Each spectrum was obtained from an average of 128 scans. An Orbis Micro X-ray Fluorescence (Micro-XRF) Analyzer with a detection limit of <5 ppm for a spot size of 30 to 40 μm using primary beam filters was used for XRF analysis in order to determine the presence of Ti and Zn in the prepared samples. TGA analysis was performed using a Mettler-Toledo TGA/DSC STAR System to investigate the amount of titanium (wt %) in each prepared sample. High Resolution TEM (HRTEM) analysis equipped with energy dispersive X-ray Spectroscopy (EDX) was conducted using a FEI

Titan Microscope operating at 300 KeV for the microscopic morphological observation of Ti/NCs and Ti/AC and for the confirmation of the existence of Ti without any Zn. Samples for HRTEM analysis were prepared using a suspension in acetone and dropped onto a copper grid with holey carbon support then dried overnight under vacuum. Particle size distributions of Ti particles in both the Ti/NC and Ti/AC samples were evaluated using the Feret function of ImageJ 1.46 software. Elemental analysis was performed on a Perkin Elmer Optima 3300XL ICP-OES. External titanium standards were used to generate calibration curves, and a blank calibration sample was used to subtract background signal.

3. RESULTS AND DISCUSSION

3.1. Materials Characterization. Successful postsynthetic modification of IRMOF-3 with Ti(O-*i*Pr)$_4$ (IRMOF-3/Ti) was verified via physisoportion, ICP-OES, SEM, XRD, FT-IR, XRF, and TGA. The microporous characteristics as well as the macroscopic morphology of IRMOF-3 and IRMOF-3/Ti were analyzed via N_2 physisorption and the results are depicted in Figure 2 and Table 1. It was determined that despite a small

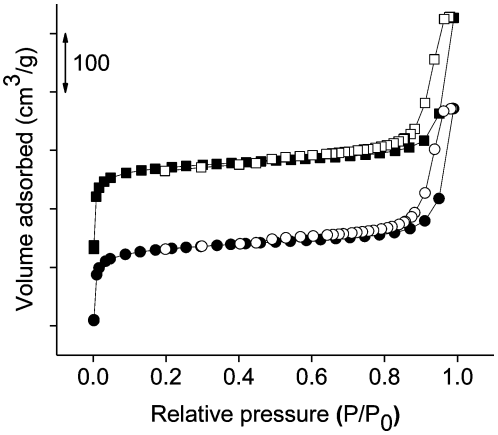

Figure 2. N_2 isotherms (adsorption (solid symbol), desorption (empty symbol)) of parent IRMOF-3 (rectangle) and IRMOF-3/Ti (circle).

Table 1. Physical Property of Prepared Materials

material	V_{meso} (cm^3/g)	V_{mjcro} (cm^3/g)	S_{BET} (m^2/g)	$S_{Langmuir}$ (m^2/g)
IRMOF-3	0.41	0.47	980	1370
IRMOF-3/Ti	0.38	0.38	870	1200
Ti/NC	1.19	0.35	1060	1330
AC	0.28	0.47	880	1100
Ti/AC	0.45	0.25	790	990

decrease in mesopore volume, micropore volume, and surface area after postsynthetic modification, these characteristics of the IRMOF-3/Ti material were well-maintained after postsynthetic modification. The slight decrease in pore volume and surface area observed was due to the occupancy of micropores by -Ti(O-*i*Pr)$_3$ coordinated with the amine functionality of IRMOF-3.

XRD patterns of IRMOF-3 before and after postsynthetic modification with Ti(O-*i*Pr)$_4$ are shown in Figure 3. The XRD pattern of IRMOF-3 matched the pattern reported in literature which indicated the presence of the crystalline MOF structure.[37] IRMOF-3/Ti exhibited the same prominent peaks as the unmodified IRMOF-3, which indicated the postsynthetic modification of the IRMOF-3 with Ti(O-*i*Pr)$_4$ did not affect the MOF structure. Additionally, SEM imaging showed the

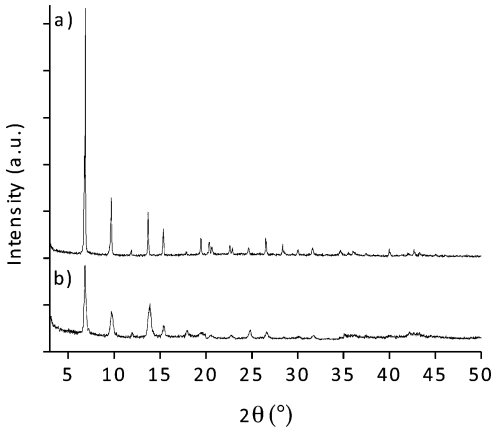

Figure 3. XRD patterns of (a) parent IRMOF-3, and (b) IRMOF-3/Ti. All major peaks were in good agreement with the predicted diffraction patterns of IRMOF-3 (CCDC No.: 738809, not shown here).

macroscopic morphology of IRMOF-3 was maintained after being subjected to postsynthetic modification with Ti(O-*i*Pr)$_4$ (see Figure S1 in the Supporting Information). The FT-IR spectrum (see Figure S2 in the Supporting Information) of IRMOF-3 showed two peaks at 3332 and 3475 cm^{-1} due to the ν(N−H) stretching of the amine functionality. The post-synthetically modified IRMOF-3 FTIR spectrum showed the presence of a ν(C−H) stretches centered at ∼2875 cm^{-1} originating from the isopropoxy group in the titanium precursor. Additionally, a peak shift of the ν(N−H) stretch (from 3332 and 3475 cm^{-1} to 3386 and 3491 cm^{-1}, respectively) after the incorporation of Ti(O-*i*Pr)$_4$ was attributed to the coordination of the titanium precursor with the amine functionality on IRMOF-3. Further evidence for the successful postsynthetic modification of IRMOF-3 was determined via ICP-OES and XRF, both of which showed the presence of Ti in the material. The Ti content of IRMOF-3/Ti, as measured by ICP-OES, was 0.2 wt %. As a control, IRMOF-1, which is iso-structural to IRMOF-3 except it lacks the primary amine functionality, was postsynthetically modified with Ti(O-*i*Pr)$_4$ using an identical procedure as IRMOF-3. The Ti content of postsynthetically modified IRMOF-1 was measured by both XRF and ICP-OES, and it was found that without the amine functionality, Ti was not incorporated into the MOF structure. This control experiment further suggested Ti(O-*i*Pr)$_3$-amine coordination was present in the postsynthetically modified IRMOF-3 sample.[25] From ICP-OES analysis, postsynthetically modified IRMOF-3 contained 0.012 of Ti precursor per amine functionality. Postsynthetically modified IRMOF-3 with a higher Ti to amine ratio, however, was difficult to obtain because of the diffusion limitation of Ti(O-*i*Pr)$_4$ caused by the small pore size of IRMOF-3 (12-13 Å).[25,26]

The CCR method was applied to IRMOF-3/Ti at a temperature of 1000 °C, and the resulting material (denoted as Ti/NC) was characterized by a battery of techniques. From XRF analysis, Zn was not detected in the sample after CCR, indicating complete removal of the Zn species. The Ti/NC material was then analyzed by TGA (see Figure S3 in the Supporting Information) under air flow in order to determine the Ti content as well as its thermal stability. The weight of Ti in the material was first determined by assuming the weight of the remaining material after complete combustion (>900 °C) was solely composed of TiO_2. The weight percentage of Ti in

the material was then calculated by using this final weight value in conjunction with the initial weight of the material (taken to be the weight value before the onset of combustion) and was found to be 4.3 wt % Ti. Furthermore, TGA results demonstrated the increased thermal stability of the Ti/NC material, as it did not undergo combustion until a temperature >400 °C, whereas the parent IRMOF-3/Ti material began to degrade as early as 200 °C. HRTEM images were taken of the Ti/NC material and are depicted in Figure 4. Analysis of the

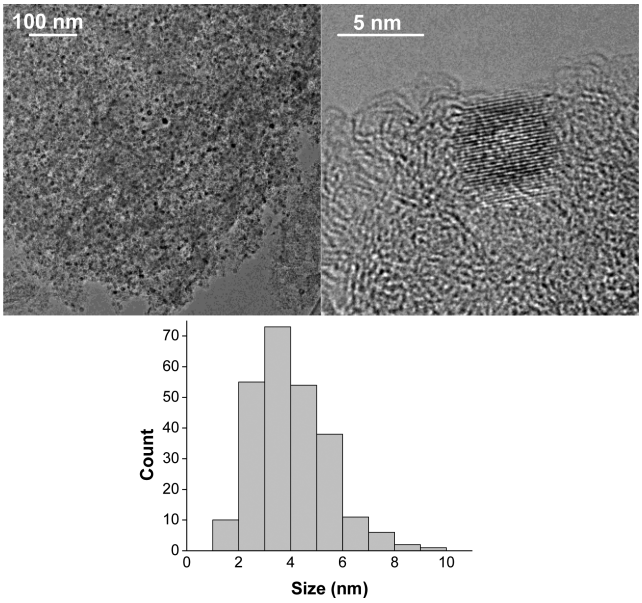

Figure 4. HRTEM images of Ti/NC at (top left) low and (top right) high magnification. Histogram (bottom) of the size of metal oxide particles present on Ti/NC material. The average particle size was estimated at 4 ± 1.4 nm (n = 250).

images revealed Ti/NC was composed of crystalline nanoparticles (as evidenced by the observed lattice fringes) supported on carbon. Furthermore, a survey of 250 of the crystalline nanoparticles exhibited an average size of ~4 nm on the NC surface.

The microporous and mesoporous characteristics of Ti/NC were analyzed via N_2 physisorption (Figure 5 and Table 1). The material showed a type I isotherm which indicated the

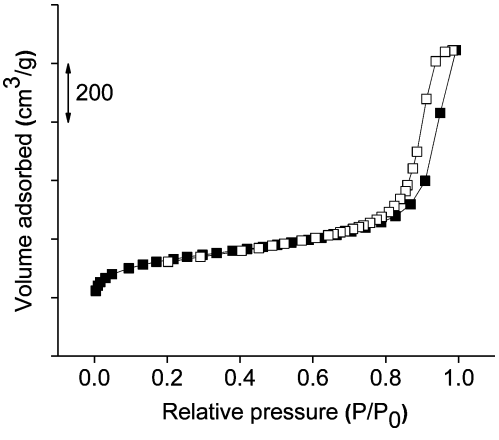

Figure 5. N_2 isotherm (adsorption (solid symbol), desorption (empty symbol)) of Ti/NC.

existence of micropores and a type IV isotherm which indicated the existence of mesopores. The mesopore volume of Ti/NC (1.19 cm^3/g) was found to be much larger than that of IRMOF-3 (0.41 cm^3/g), whereas micropore volume of Ti/NC was decreased only a slight amount (from 0.47 to 0.35 cm^3/g) after postsynthetic modifciation followed by CCR. The BET surface area of Ti/NC was found to be ~1060 m^2/g, which was greater than that of the parent IRMOF-3 at ~980 $m^2\ g^{-1}$. This was attributed to the MOF structure, which acted as a nanoporous carbon template during the degradation process.[33]

The electronic properties of the titanium species in Ti/NC were characterized via XPS, and the results are exhibited in Figure 6. It should be noted that all samples characterized by

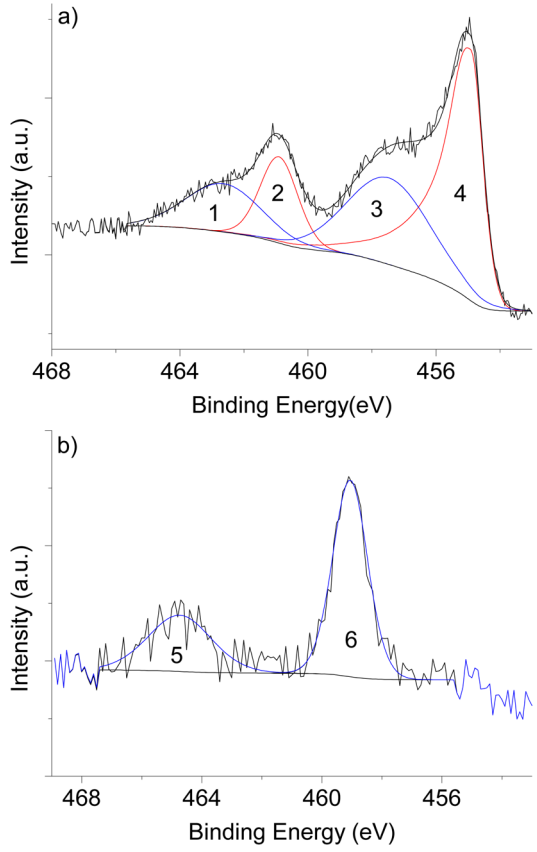

Figure 6. XPS spectra showing the Ti 2p energy region for (a) Ti/NC and (b) Ti/AC. Fitted regions refer to the following states: 1, Ti_2O_3 $2p_{1/2}$; 2, TiO $2p_{1/2}$; 3, Ti_2O_3 $2p_{3/2}$; 4, TiO $2p_{3/2}$; 5, TiO_2 $2p_{1/2}$; and 6, TiO_2 $2p_{3/2}$.

XPS had been stored under air for the same amount of time before analysis (approximately one week). The XPS spectrum of the Ti 2p energy for Ti/NC showed two Ti $2p_{3/2}$ peaks at binding energies (BE) of 455.1 and 457.7 eV, which corresponded with Ti oxide phases of TiO (Ti^{II}) and Ti_2O_3 (Ti^{III}), respectively.[38] The change in oxidation state of the coordinated Ti(O-iPr)$_4$ (Ti^{IV}) in the parent IRMOF-3/Ti to the Ti^{II} and Ti^{III} states occurred because of carbothermal reduction of Ti during the CCR method.

As a control material to substantiate the novelty of this preparation method, titanium oxide supported on activated carbon (Ti/AC) was synthesized via a conventional incipient wetness technique, and its properties were investigated. The motivation for this study stemmed from the idea that the thermally rigid coordination bond between Ti(O-iPr)$_4$ and the

amine functionality in IRMOF-3 could minimize the aggregation of titanium oxide during its thermal decomposition leading to smaller, more dispersed active sites and a subsequently more active catalyst. This was corroborated by HRTEM images, depicted in Figure 7, which showed the Ti/AC material (on a holey carbon support) contained nanoparticles on an AC support. Size analysis revealed the average diameter of the particles to be ~29 nm. N_2 physisorption (see Figure S4 in the Supporting Information and Tabel 1) analysis showed a mesopore volume of 0.45 cm^3/g, a micropore volume of 0.25 m^2/g, and BET surface area of 790 m^2/g, all of which were significantly lower than the MOF-templated Ti/NC material. The XPS spectrum (Figure 6b) of the Ti/AC material showed a Ti $2p_{3/2}$ peak at a BE of 459.1 eV, which corresponded to a TiO_2 phase (Ti^{IV}),[38] further exhibiting the ability of the novel CCR method to synthesize unique materials (Ti^{II}, Ti^{III} for Ti/NC).

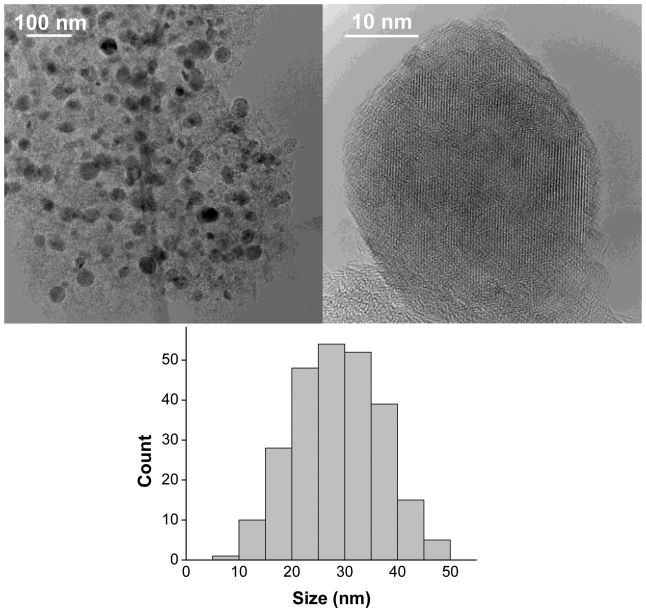

Figure 7. HRTEM images of Ti/AC at (top left) low and (top right) high magnification. Histogram (bottom) of the size of metal oxide particles present on Ti/AC material. The average particle size was estimated at 29 ± 8.4 nm (n = 250).

3.2. Catalysis Studies on the Oxidation of Dibenzothiophene. The novel Ti/NC along with its parent materials and Ti/AC were then tested for catalytic activity and stability in the oxidation of dibenzothiophene (DBT) by *tert*-butyl hydroperoxide (TBHP). In this reaction, the sulfur atom of dibenzothiophene is first oxidized to yield the corresponding sulfoxide and then subsequently oxidized again resulting in the sulfone (Scheme 1). The Ti/NC catalyst was expected to show activity in this reaction, as it has been shown that Ti-based materials catalyze oxidation reactions through the addition of an organic peroxide to the coordinatively unsaturated tetrahedral metal centers.[23,39]

Scheme 1. Reaction Schematic for the Oxidation of Dibenzothiophene

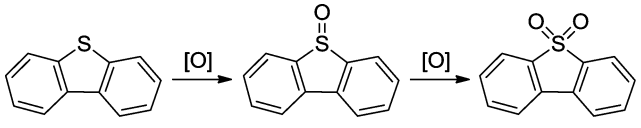

The apparent reaction rate constant values (k_{app}) were obtained by fitting experimental data to a pseudo-first-order model. As shown in Figure 8 and Table 2, unmodified IRMOF-3 showed activity (k_{app} = 0.4 × 10^{-3} min^{-1}) comparable to a blank reaction with no added catalyst, which was expected because this sample contained no Ti. Postsynthetically modified IRMOF-3/Ti did indeed show enhanced activity (k_{app} = 3.0 × 10^{-3} min^{-1}) over unmodified IRMOF-3 but suffered from poor stability as XRD analysis (see Figure S5 in the Supporting Information) of the spent catalyst showed a loss in the crystallinity of the IRMOF-3 structure after reaction. The instability of IRMOF-3/Ti could be ascribed to its weak bonds, which are chemically vulnerable to a strong oxidant such as TBHP.

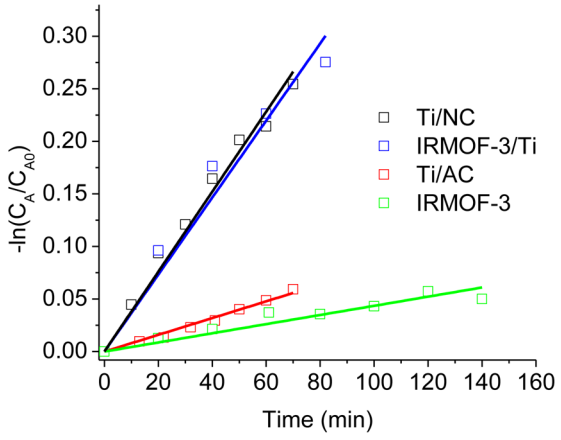

Figure 8. Fitting of experimental data to a pseudo-first-order rate model in the oxidation of dibenzothiophene catalyzed by various prepared materials. Reaction conditions: 9 μmol of Ti, 3.5 mmol of DBT (substrate), 30 mL of decane (solvent), 0.5 mL of dodecane (internal standard), 7.5 mmol of *tert*-butyl hydroperoxide (TBHP, oxidant), 100 °C (reaction temperature), ambient pressure under air.

Table 2. Catalytic Activity of Prepared Materials in the Oxidation of DBT by TBHP

entry	material[a]	k_{app} (min^{-1}) × 10^{3}[b]
1	IRMOF-3	0.4
2	IRMOF-3/Ti	3.0
3	Ti/NC	3.4
4	Ti/AC	0.8

[a]Reaction conditions: 9 μmol of Ti, 3.5 mmol of DBT (substrate), 30 mL of decane (solvent), 0.5 mL of dodecane (internal standard), 7.5 mmol of *tert*-butyl hydroperoxide (TBHP, oxidant), 100 °C (reaction temperature), ambient pressure under air. [b]The k_{app} (apparent reaction rate constant) values were obtained by fitting the experimental data to a pseudo-first-order model.

The Ti/AC catalyst enhanced the reaction rate (k_{app} = 0.8 × 10^{-3} min^{-1}) over unmodified IRMOF-3, but had a significantly lower reaction rate constant than IRMOF-3/Ti. This was attributed to the lower dispersion of active sites (large nanoparticles, ~29 nm) on Ti/AC when compared to the single-site tethering found in the IRMOF-3/Ti material. Contrary to the Ti/AC material, Ti/NC exhibited excellent performance in catalytic activity (k_{app} = 3.4 × 10^{-3} min^{-1}), outperforming even the IRMOF-3/Ti material.

Recycle tests (Figure 9) were then performed on Ti/AC and Ti/NC in order to evaluate stability of these materials. The Ti/

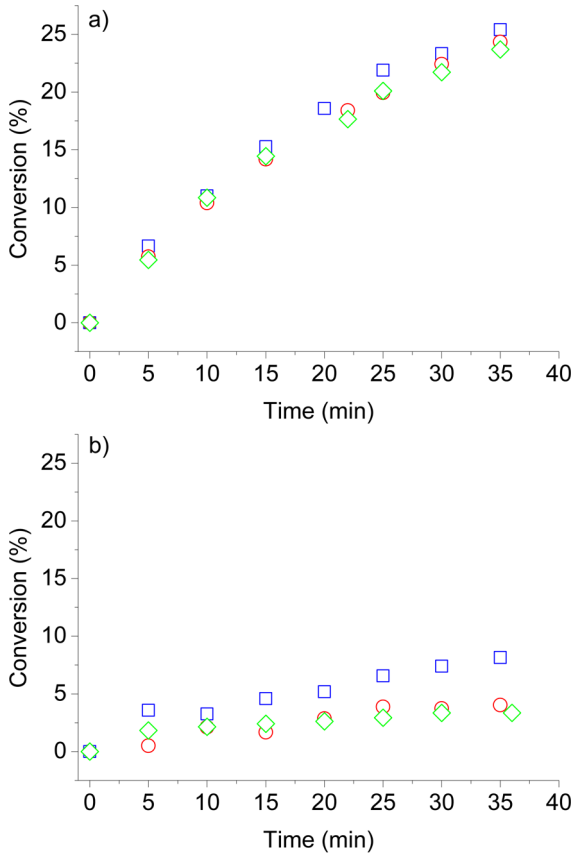

Figure 9. Recycle data for the oxidation of DBT using TBHP catalyzed by (a) Ti/NC and (b) Ti/AC after (blue square) one, (red circle) two, and (green diamond) three consecutive reactions. Reaction conditions: 36 μmol of Ti (initial reaction), 3.5 mmol of DBT (substrate), 30 mL of decane (solvent), 0.5 mL of dodecane (internal standard), 7.5 mmol of tert-butyl hydroperoxide (TBHP, oxidant), 100 °C (reaction temperature). After each run, the catalyst was filtered and washed with N,N-dimethylformamide and chloroform, collected, and dried in a vacuum oven at 40 °C overnight. In each run, the same reaction conditions were consistently employed.

AC material lost a great deal of activity on subsequent recycle tests. This loss of activity was initially thought to be caused by leaching of active sites but ICP-OES analysis of the filtrate showed all materials only lost <1% of Ti after a reaction. The activity loss could potentially be due to difficulty in collecting sample between consecutive reactions. SEM analysis (see Figure S6 in the Supporting Information) of the Ti/AC material showed carbon support particle sizes of 0.18-5.61 μm making it difficult to collect and recycle by simple filtration. Recycle tests on the Ti/NC material showed that it retained its high catalytic activity even after multiple catalytic reactions (Figure 9a). Additionally, the Ti/NC material was more easily separated from the reactant mixture, allowing for more subsequent recycle reactions, possibly because of the larger particle size of the carbon support (0.5−1 mm) as determined by SEM (see Figure S7 in the Supporting Information).

To elucidate the source of catalytic activity in Ti/NC as compared to Ti/AC, the Ti/NC material was oxidized by calcination in air at 350°C for 1 h and then used for catalysis. Catalytic tests under identical conditions showed the calcined Ti/NC material obtained a slower reaction rate constant (k_{app} = 2.5 × 10^{-3} min^{-1}) than the uncalcined material. XPS analysis (Figure 10) revealed that the calcined material retained the peak corresponding to Ti^{III} but the Ti^{II} peak disappeared and was replaced by a higher BE peak attributed to Ti^{IV}.

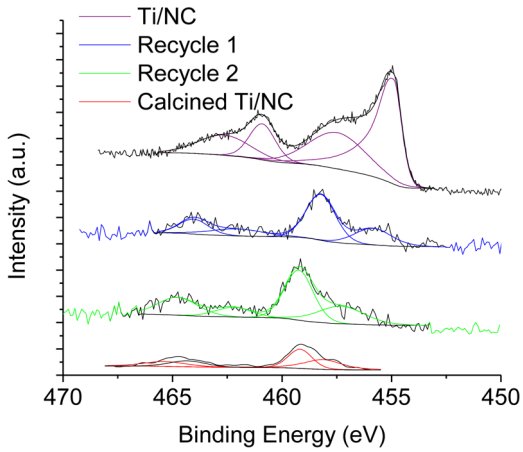

Figure 10. XPS spectra showing the Ti 2p energy region for Ti/NC (reprinted from Figure 6a), calcined Ti/NC, and Ti/NC after the 1st and 2nd recycle reactions. The shift left to higher binding energies indicates oxidation of the Ti species.

TEM analysis (Figure 11) of the calcined Ti/NC material showed sintering of nanoparticles occurred during calcination

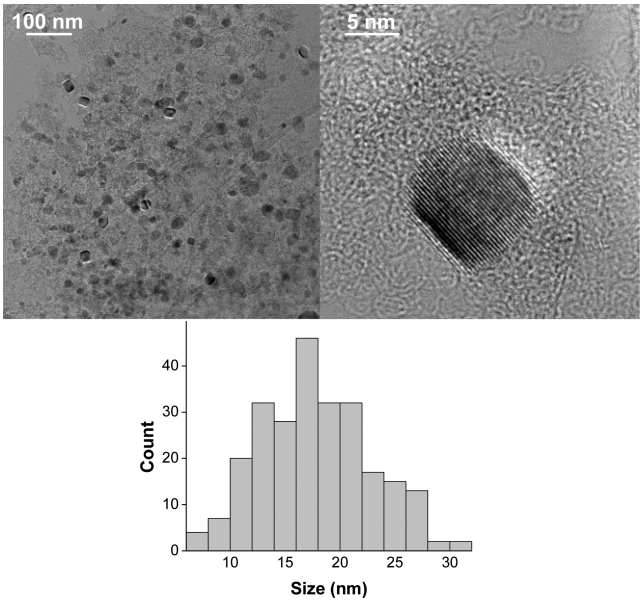

Figure 11. HRTEM images of Ti/NC after calcination (air, 5 °C/min, 350 °C for 1 h) at low (top left) and high (top right) magnification. Histogram (bottom) of the size of titanium oxide particles present on this sample. The average particle size was estimated at 18 ± 4.9 nm (n = 250).

resulting in an average nanoparticle size of ∼18 nm. The source of high activity of the Ti/NC material over Ti/AC, however, was attributed to nanoparticle size rather than oxidation state as the Ti/NC material used during recycle reactions showed a shift to more oxidized states in XPS but retained its catalytic activity (Figures 9 and 10). Thus, the high catalytic activity and

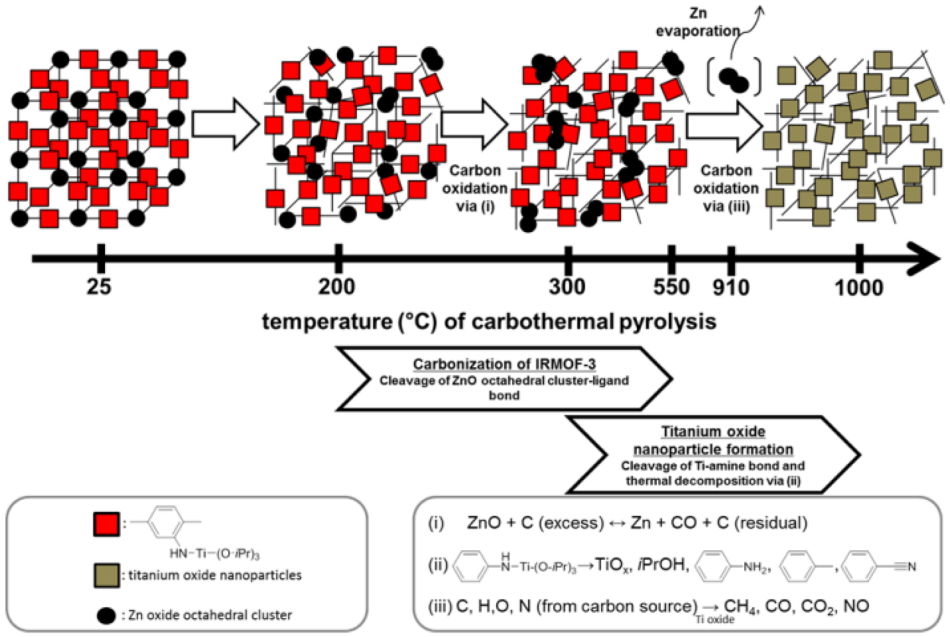

Figure 12. Proposed mechanism for the formation of Ti/NC.

stability were attributed to the highly-dispersed small nanoparticles (~4 nm) on Ti/NC as compared with Ti/AC and the strong metal oxide-support interaction derived from the CCR method, respectively. These results demonstrated the value of Ti/NC as an active and stable catalyst for oxidation reactions.

3.3. Proposed Mechanism for the Formation of Ti/NC.

Characterization results of the various prepared materials allowed for a proposed mechanism for the formation of Ti/NC to be suggested (Figure 12). The carbonization of IRMOF-3 is initiated by the cleavage of the bond between the zinc oxide octahedral cluster and the organic linker. This carbonization step was simultaneously accompanied by the formation of ZnO in the temperature range between 200 and 550 °C (see Figure S8 in the Supporting Information). When the IRMOF-3/Ti material was subjected to CCR at 550 °C, the resulting material contained crystalline ZnO from XRD analysis (see Figure S9 in the Supporting Information) indicating the occurrence of the previous step. As the temperature was increased above 800 °C, the ZnO was reduced to Zn metal via carbothermal reduction which led to the continuous consumption of the carbon source until the evaporation of Zn occurred at >910 °C (see Figure S10 in the Supporting Information).[33] Concurrently, titanium oxide nanoparticles were produced via thermal decomposition initiated by the cleavage of the coordinate bond between the titanium precursor [−Ti(O-*i*Pr)$_3$] and the amine functionality (−NH$_2$−) of the organic linker in IRMOF-3 above 300 °C, which is plausible on the basis of the work by Tilley and coworkers with Ti complexes on silica.[40−42] The cleaved fragments of titanium precursor then thermally decomposed via pyrolysis and carbothermal reduction[43,44] to form titanium oxide nanoparticles. Further evidence supporting cleavage of the Ti complex from the MOF was seen in GC/MS results (see Figure S11 in the Supporting Information) of pyrolyzed IRMOF-3/Ti, which showed the formation of isopropanol derived from -Ti(O-*i*Pr)$_3$ thermal decomposition and aniline derived from organic linker degradation. These Ti oxide nanoparticles could then undergo further carbothermal reduction leading to additional carbon consumption. This type of carbon consumption presumably could give rise to the formation of concave holes for stronger immobilization of the titanium oxide nanoparticles to prevent their aggregation at high temperature (i.e. 1000 °C).[45] This occurrence was envisioned when considering the smaller nanoparticle sizes of Ti/NC (~4 nm) as compared to Ti/AC nanoparticles (Figure 7, ~29 nm) prepared via incipient wetness impregnation. As a result of this synthetic process, the CCR method was able to produce unique materials that were highly stable and active for this oxidation reaction.

4. CONCLUSION

In this work, a novel synthetic method was used to prepare titanium oxide nanoparticles supported on amorphous carbon with nanoporosity (Ti/NC). This was achieved by post-synthetically modifying IRMOF-3 via coordination of the pendant amine functionality with Ti(O-*i*Pr)$_4$ followed its carbothermal pyrolysis. In this method, the MOF structure acted as a template for the formation of nanoporous carbon during the carbonization procedure, while the Ti metal was simultaneously carbothermally reduced. The synthesized Ti/NC material was characterized using a number of techniques revealing the Ti/NC material was composed of well-dispersed, crystalline titanium oxide nanoparticles supported on carbon that were much smaller (~4 nm) and in a more reduced oxidation stated (Ti^{II}, Ti^{III}) than titanium oxide particles supported on activated carbon (Ti/AC) prepared via conventional incipient wetness impregnation (~29 nm, Ti^{IV}). N$_2$ physisorption and TGA analysis were used to show the Ti/NC material possessed a surface area, mesopore volume, and thermal stability even greater than its parent IRMOF-3. The novel Ti/NC material was tested for catalytic activity amd with its parent materials (IRMOF-3 and IRMOF-3/Ti) along with Ti/AC in the oxidation of DBT. The Ti/NC material was shown to be a promising oxidation catalyst as it exhibited a much higher catalytic activity (at k_{app} = 3.4 × 10^{-3} min^{-1}) than all other tested materials under identical reaction conditions. Furthermore, the Ti/NC material possessed a high stability under catalytic conditions by retaining its catalytic activity even

after multiple recycle reactions. A formation mechanism, deduced by studying different synthetic conditions, was also proposed that discusses the roles of both Zn and Ti in the preparation of Ti/NC. It was proposed that carbonization was initiated by the cleavage of the Zn oxide octahedral clusters from the organic linkers (200−550 °C) followed by carbothermal reduction of Zn oxide (>800 °C) and subsequent Zn metal evaporation (>910 °C). During a concurrent step, the coordinate bond between the organometallic Ti precursor and the amine functionality of the IRMOF-3 ligand was broken (>300 °C). The Ti precursor then underwent decomposition to titanium oxide followed by carbothermal reduction. In this work the CCR method was used to prepare carbon supported titanium oxide nanoparticles, but it could easily be applied to a number of other postsynthetically MOFs resulting in a multitude of different materials. Work is currently in progress to prepare and characterize such materials.

■ ASSOCIATED CONTENT

Ⓢ Supporting Information

FT-IR spectra of IRMOF-3 and IRMOF-3/Ti; TGA profiles for IRMOF-3, IRMOF-3/Ti, and Ti/NC in air; N_2 physisorption isotherms for AC and Ti/AC; XRD patterns of IRMOF-3/Ti before and after catalysis; SEM image of Ti/AC; TGA profile of IRMOF-3 in N_2; XRD pattern of IRMOF-3/Ti after pyrolysis at 550 °C, N_2 physisorption isotherm and TGA profile for IRMOF-3/Ti after pyrolysis at 550 °C; and GC trace for the pyrolysis of IRMOF-3/Ti. This material is available free of charge via the Internet at http://pubs.acs.org.

■ AUTHOR INFORMATION

Corresponding Author

*E-mail: jhicks3@nd.edu. Fax: (+1) 574-631-8366.

Author Contributions

‡Authors J.K. and N.D.M. contributed equally.

Notes

The authors declare no competing financial interest.

■ ACKNOWLEDGMENTS

We thank the National Science Foundation (NSF) for partial support through the BRIGE program (CBET-1125145). We also thank the Center for Sustainable Energy at Notre Dame, the Center for Environmental Science and Technology at Notre Dame, and the Notre Dame Integrated Imaging Facilities for partial support through access to their facilities and instrumentation.

■ REFERENCES

(1) Rodriguez-Reinoso, F. *Carbon* **1998**, *36*, 159−175.
(2) Calvino-Casilda, V.; López-Peinado, A. J.; Durán-Valle, C. J.; Martín-Aranda, R. M. *Cat. Rev.: Sci. Eng.* **2010**, *52*, 325−380.
(3) Xia, B. Y.; Wang, J. N.; Wang, X. X.; Niu, J. J.; Sheng, Z. M.; Hu, M. R.; Yu, Q. C. *Adv. Funct. Mater.* **2008**, *18*, 1790−1798.
(4) Wang, L.; Tian, C.; Zhang, H.; Fu, H. *Eur. J. Inorg. Chem.* **2012**, *2012*, 961−968.
(5) Delannoy, L.; El Hassan, N.; Musi, A.; Nguyen Le To, N.; Krafft, J.-M.; Louis, C. *J. Phys. Chem. B* **2006**, *110*, 22471−22478.
(6) Yang, Y.; Chiang, K.; Burke, N. *Catal. Today* **2011**, *178*, 197−205.
(7) Quinn, B. M.; Dekker, C.; Lemay, S. G. *J. Am. Chem. Soc.* **2005**, *127*, 6146−6147.
(8) Tanaka, N.; Nishikiori, H.; Kubota, S.; Endo, M.; Fujii, T. *Carbon* **2009**, *47*, 2752−2754.
(9) Koltypin, Y.; Fernandez, A.; Rojas, T. C.; Campora, J.; Palma, P.; Prozorov, R.; Gedanken, A. *Chem. Mat.* **1999**, *11*, 1331−1335.
(10) Zhu, S.; Zhou, H.; Hibino, M.; Honma, I.; Ichihara, M. *Adv. Funct. Mater.* **2005**, *15*, 381−386.
(11) Lin, Y.; Watson, K. A.; Fallbach, M. J.; Ghose, S.; Smith, J. G.; Delozler, D. M.; Cao, W.; Crooks, R. E.; Connell, J. W. *ACS Nano* **2009**, *3*, 871−884.
(12) Dhakshinamoorthy, A.; Alvaro, M.; Garcia, H. *Catal. Sci. Technol.* **2011**, *1*, 856−867.
(13) Farha, O. K.; Hupp, J. T. *Acc. Chem. Res.* **2010**, *43*, 1166−1175.
(14) Bae, Y. S.; Lee, C. Y.; Kim, K. C.; Farha, O. K.; Nickias, P.; Hupp, J. T.; Nguyen, S. T.; Snurr, R. Q. *Angew. Chem., Int. Ed.* **2012**, *51*, 1857−1860.
(15) Dubbeldam, D.; Galvin, C. J.; Walton, K. S.; Ellis, D. E.; Snurr, R. Q. *J. Am. Chem. Soc.* **2008**, *130*, 10884−10885.
(16) Han, S. S.; Deng, W. Q.; Goddard, W. A., 3rd *Angew. Chem., Int. Ed.* **2007**, *46*, 6289−6292.
(17) Herm, Z. R.; Wiers, B. M.; Mason, J. A.; van Baten, J. M.; Hudson, M. R.; Zajdel, P.; Brown, C. M.; Masciocchi, N.; Krishna, R.; Long, J. R. *Science* **2013**, *24*, 960−964.
(18) Sun, F.; Yin, Z.; Wang, Q. Q.; Sun, D.; Zeng, M. H.; Kurmoo, M. *Angew. Chem., Int. Ed.* **2013**, *52*, 4538−4543.
(19) Thompson, J. A.; Brunelli, N. A.; Lively, R. P.; Johnson, J. R.; Jones, C. W.; Nair, S. *J. Phys. Chem. C* **2013**, *117*, 8198−8207.
(20) Gascon, J.; Aktay, U.; Hernandezalonso, M.; Vanklink, G.; Kapteijn, F. *J. Catal.* **2009**, *261*, 75−87.
(21) Corma, A.; Garcia, H.; Llabres i Xamena, F. X. *Chem. Rev.* **2010**, *110*, 4606−4655.
(22) Farrusseng, D.; Aguado, S.; Pinel, C. *Angew. Chem., Int. Ed.* **2009**, *48*, 7502−7513.
(23) McNamara, N. D.; Neumann, G. T.; Masko, E. T.; Urban, J. A.; Hicks, J. C. *J. Catal.* **2013**, *305*, 217−226.
(24) Stock, N.; Biswas, S. *Chem. Rev.* **2012**, *112*, 933−969.
(25) Kim, J.; Kim, D. O.; Kim, D. W.; Park, J.; Jung, M. S. *Inorg. Chim. Acta* **2012**, *390*, 22−25.
(26) Kim, J.; Kim, D. O.; Kim, D. W.; Sagong, K. *J. Solid State Chem.* **2013**, *197*, 261−265.
(27) Pintado-Sierra, M.; Rasero-Almansa, A. M.; Corma, A.; Iglesias, M.; Sánchez, F. *J. Catal.* **2013**, *299*, 137−145.
(28) Bloch, E. D.; Britt, D.; Lee, C.; Doonan, C. J.; Uribe-Romo, F. J.; Furukawa, H.; Long, J. R.; Yaghi, O. M. *J. Am. Chem. Soc.* **2010**, *132*, 14382−14384.
(29) Song, Y. F.; Cronin, L. *Angew. Chem., Int. Ed. Engl.* **2008**, *47*, 4635−4637.
(30) Nelson, A. P.; Farha, O. K.; Mulfort, K. L.; Hupp, J. T. *J. Am. Chem. Soc.* **2008**, *131*, 458−460.
(31) Farha, O. K.; Hupp, J. T. *Acc. Chem. Res.* **2010**, *43*, 1166−1175.
(32) Jiang, H. L.; Liu, B.; Lan, Y. Q.; Kuratani, K.; Akita, T.; Shioyama, H.; Zong, F.; Xu, Q. *J Am Chem Soc* **2011**, *133*, 11854−11857.
(33) Liu, B.; Shioyama, H.; Akita, T.; Xu, Q. *J. Am. Chem. Soc.* **2008**, *130*, 5390−5391.
(34) Liu, B.; Shioyama, H.; Jiang, H.; Zhang, X.; Xu, Q. *Carbon* **2010**, *48*, 456−463.
(35) Su, P.; Xiao, H.; Zhao, J.; Yao, Y.; Shao, Z.; Li, C.; Yang, Q. *Chem. Sci.* **2013**, *4*, 2941−2946.
(36) Eddaoudi, M.; Kim, J.; Rosi, N.; Vodak, D.; Wachter, J.; O'Keeffe, M.; Yaghi, O. M. *Science* **2002**, *295*, 469−472.
(37) Millward, A. R.; Yaghi, O. M. *J. Am. Chem. Soc.* **2005**, *127*, 17998−17999.
(38) McCafferty, E.; Wightman, J. P. *Surf. Interface. Anal.* **1998**, *26*, 549−564.
(39) Kim, S.-N.; Kim, J.; Kim, H.-Y.; Cho, H.-Y.; Ahn, W.-S. *Catal. Today* **2013**, *204*, 85−93.
(40) Brutchey, R. L.; Ruddy, D. A.; Andersen, L. K.; Tilley, T. D. *Langmuir* **2005**, *2005*, 9567−9583.
(41) Jarupatrakorn, J.; Tilley, T. D. *J. Am. Chem. Soc.* **2002**, *124*, 8380−8388.

(42) Brutchey, R. L.; Mork, B. V.; Sirbuly, D. J.; Yang, P.; Tilley, T. D. *J. Mol. Catal. A: Chem.* **2005**, *238*, 1−12.
(43) Zhang, H.; Li, F.; Jia, Q.; Ye, G. *J. Sol−Gel Sci. Technol.* **2008**, *46*, 217−222.
(44) Koc, R. *J. Mater. Sci.* **1998**, *33*, 1049−1055.
(45) Song, Q.; Cai, J.; Zhang, J.; Yu, W.; Wang, F.; Xu, J. *Chin. J. Catal.* **2013**, *34*, 651−658.